Reduction of 1+1 resonance enhanced MPI spectra to populations and alignment factors

D. C. Jacobs and R. N. Zare
Department of Chemistry, Stanford University, Stanford, California 94305

(Received 14 July 1986; accepted 6 August 1986)

A theory is presented to reduce 1 + 1 resonance enhanced multiphoton ionization (REMPI) spectra to accurate rovibrational state population distributions. Classical and quantum mechanical treatments are developed to model the polarization dependence of the REMPI signal from an initially aligned ground state having cylindrical symmetry. The theory includes the effects of saturation and intermediate state alignment. It is demonstrated that, for favorable cases, 1 + 1 REMPI allows the determination of the relative population as well as the quadrupole and hexadecapole moments of the alignment for rovibrational levels of a linear molecule. The classical treatment differs from that of the quantum treatment by less than 5% for rotational quantum numbers greater than $J = 4$, suggesting that the classical treatment suffices for 1 + 1 REMPI in most molecular systems.

I. INTRODUCTION

Resonance enhanced multiphoton ionization (REMPI) is a very sensitive technique for the gas-phase detection of many molecules.[1] With a simple time-of-flight collection scheme, the created ions can be mass selected and counted with near unit efficiency, while background interference can be almost completely suppressed. In addition to providing useful spectroscopic information about neutral molecules and their ions, the REMPI technique can be utilized to determine internal state population distributions. A number of research investigations have exploited this aspect to study the dynamics of gas–gas[2–4] and gas–surface[5,6] scattering processes.

The ability to extract relative state populations from REMPI spectra of linear molecules relies heavily on an understanding of the effects of both "intermediate state alignment" and "saturation" on the observed ion signal. In a recent study of 1 + 1 REMPI on the NO $A\ ^2\Sigma^+$–$X\ ^2\Pi$ system, Booth, Bragg, and Hancock[7] observed an enhancement of P and R branch members over their Q counterparts. They proposed a classical model based on an intermediate state alignment effect which succeeded in giving a qualitative explanation for the observed phenomena. The intermediate state alignment effect can be thought of in the following manner. Suppose a beam of linearly polarized light is incident on an isotropic distribution of ground state molecules (i.e., all M sublevels within a given J level are equally populated). The intermediate state will be effectively aligned through the preferential excitation of those molecules having larger projections of the transition dipole moment on the electric field vector of the linearly polarized light beam. Ionization efficiency of the intermediate state can also be M dependent, and thus the degree of anisotropy created in the intermediate state can affect the overall MPI ion production.

However, the treatment by Booth, Bragg, and Hancock[7] does not consider saturation. Saturation in REMPI can refer to either a substantial population transfer from the ground state to the resonant intermediate state, or a complete or near complete conversion of the resonant intermediate state into ions. In 1 + n REMPI, saturation of the resonant step is often a concern, because the cross section of a resonant transition is usually greater than that of a transition to the ion continuum, thus favoring stimulated emission over ionization for depopulation of the intermediate state.

This paper presents both classical and quantum expressions for relating REMPI ion intensities of linear molecules to ground state populations and alignment. These treatments include the interdependent effects of saturation and intermediate state alignment. The derivation of population information from REMPI spectra is most ideal under situations where there is one-photon resonant excitation followed by one-photon ionization. One-photon processes are more facile than multiple-photon excitations and are less affected by spatial and temporal inhomogeneities in the laser beam profile. One-photon transitions also avoid accidental resonances or near resonances between virtual and real states which often occur in coherent multiphoton transitions giving complicated enhancements and Stark shifts to portions of the spectra.[8,9] This paper will thus limit its discussion to 1 + 1 REMPI for the latter reasons, although one may modify the conclusions to treat other $m + n$ systems. In addition, the following refers to the behavior of isolated molecules at low pressures where collision effects as well as the competition between REMPI and nonlinear optical mixing may be neglected.[8,9] Ionization will only be treated through a direct mechanism; autoionization can cause enhancements that will impair our ability to extract accurate population information.

An accompanying paper[10] applies the theory developed here to the 1 + 1 REMPI of nitric oxide via the resonant NO $A\ ^2\Sigma^+$–$X\ ^2\Pi$ step. The fraction of parallel character in the ionization transition is determined and the dependence of the ion yield on the laser polarization is predicted for an initially aligned ground state.

II. THEORY

A. Saturation

A simple rate equation mode (Fig. 1) can be employed to describe the 1 + 1 REMPI system.[11–13] We examine the

 0021-9606/86/225457-12$02.10

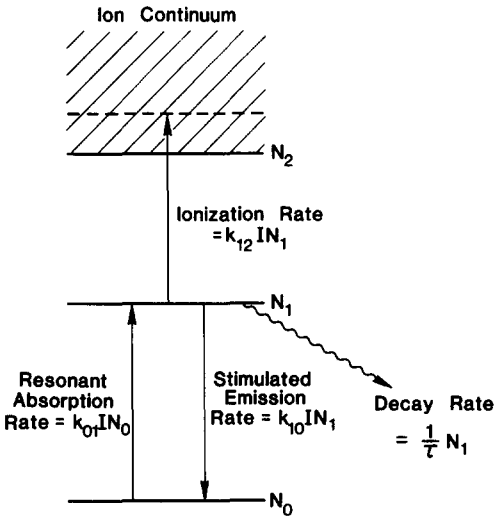

FIG. 1. Schematic diagram of 1 + 1 REMPI. Here N_0, N_1, and N_2 correspond to the populations in the ground, intermediate, and ionization states, respectively, and k_{01}, k_{10}, and k_{12} represent rate constants for the steps of resonant absorption, stimulated emission, and ionization, respectively. The intermediate state lifetime is τ.

common case where the two transitions (resonant and ionization) are excited by photons of the same color from the same source, characterized by intensity I. In reality, ionization of a specific intermediate state may produce a distribution of ion states. For the purpose of simplicity, this model treats ionization as a single rate from an intermediate state to an unspecified distribution of ion states (represented symbolically as one ion state). For a particular transition the model involves then just three states (ground, resonant intermediate, and ion) with populations N_0, N_1, and N_2, respectively. A rate model provides a more convenient description than does a density matrix formalism in cases where (1) the laser bandwidth is much larger than the natural linewidth of the resonant transition, (2) the coherence time of the laser is short relative to the Rabi flopping frequency of the resonant transition, or (3) the Rabi flopping frequency is much slower than the rate of ionization.[14,15] These conditions are met in most high intensity pulsed laser systems utilized for REMPI spectroscopy. In addition we are experimentally measuring an average quantity over many shots, where the mode quality of each shot remains undetermined. Again this makes a rate equation description very appealing.

Equations (1a)–(1c) take account of the processes of resonant excitation (absorption), stimulated emission, spontaneous emission, ionization, and any nonradiative decay from the intermediate state in order to describe the rate of change of the populations in this three-level system:

$$\frac{dN_0(t)}{dt} = -k_{01}I\,N_0(t) + k_{10}I\,N_1(t), \tag{1a}$$

$$\frac{dN_1(t)}{dt} = k_{01}I\,N_0(t) - \frac{N_1(t)}{\tau} - k_{10}I\,N_1(t) - k_{12}I\,N_1(t), \tag{1b}$$

$$\frac{dN_2(t)}{dt} = k_{12}I\,N_1(t). \tag{1c}$$

Here I corresponds to the laser intensity, τ is the intermediate state lifetime, k_{01} and k_{10} ($k_{01} = k_{10}$) are rate constants proportional to Einstein B coefficients, and k_{12} is the ionization rate constant which is proportional to the photoionization cross section. Repopulation of the ground state (v_0, J_0) through the spontaneous emission of the intermediate state (v_1, J_1) is usually a negligible effect due to the many final state pathways which are accessible to intermediate state fluorescence. We therefore omitted this term from Eq. (1a). In cases where the radiative/predissociative lifetime τ of the intermediate state is long relative to the laser pulse temporal width, the intermediate state decay term $N_1(t)/\tau$ in Eq. (1b) can also be neglected. This situation often applies to excited states of diatomic molecules, but seldom to those of polyatomic molecules.

Assuming a rectangular laser pulse of amplitude I and temporal width Δt, and initial conditions of $N_0(t=0) = N$, $N_1(t=0) = 0$, $N_2(t=0) = 0$, Eqs. (1a)–(1c) can be solved exactly[11–13] for $N_2(\Delta t)$:

$$N_2(\Delta t) = N F_{\rm sat}(k_{01},k_{12},I\Delta t), \tag{2}$$

where

$$F_{\rm sat}(k_{01},k_{12},I\Delta t) = \left(1 - \frac{1}{2B}\left\{(A+B)\exp[-\tfrac{1}{2}(A-B)I\Delta t] - (A-B)\exp[-\tfrac{1}{2}(A+B)I\Delta t]\right\}\right), \tag{3}$$

$$A = 2k_{01} + k_{12}, \tag{4a}$$

and

$$B = (4k_{01}^2 + k_{12}^2)^{1/2}. \tag{4b}$$

The quantity $N_2(\Delta t)$ describes the total number of ions produced by a laser pulse having an intensity I for a duration Δt. It can be seen that for this simplified pulse shape the ion yield depends only on the area under the pulse, $I\Delta t$, and not separately on I and Δt. Appendix A further demonstrates that within any given pulse shape, the ion yield depends only on the area under the temporal profile of the laser profile. Even in cases of moderate saturation, Appendix A shows that pulses having differing temporal shapes but the same integrated intensity result in ion yields that differ by only a small amount from that given in Eq. (2). Therefore in 1 + 1 REMPI, a real (nonrectangular) pulse can be approximated as a rectangular pulse having an equivalent integrated laser intensity $I\Delta t$.

B. REMPI transition rate constants: Classical approach

Using Fermi's Golden Rule, the transition probability for a one-photon transition is proportional to $\langle \boldsymbol{\mu}\cdot\mathbf{E}\rangle^2$ where $\boldsymbol{\mu}$ is the transition dipole moment in the molecule-fixed frame and $\mathbf{E}$ is the polarization vector in the space-fixed frame. We restrict ourselves to linearly polarized light and define the space-fixed Z axis to be along $\mathbf{E}$. For a linear molecule in the classical limit, $\boldsymbol{\mu}$ can point in two directions: either along the angular momentum vector $\mathbf{J}$ for a Q branch ($\Delta J = 0$) or in the plane of rotation for a P or R branch ($\Delta J = \mp 1$). For parallel transitions (Σ–Σ, Π–Π, etc.) only P and R branches have intensity in the classical limit; where-

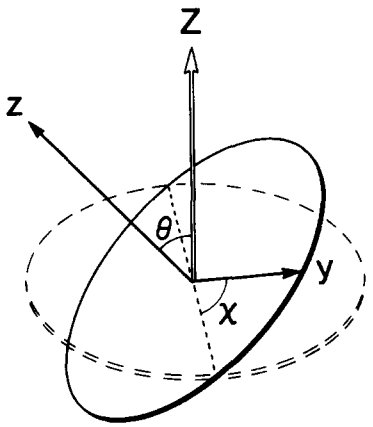

FIG. 2. Relation between the space-fixed and the molecular frames. The laser polarization vector is defined to be along the Z axis. The molecule is rotating such that its angular momentum vector points along z. The y axis is shown to lie along the transition dipole moment when the latter is located in the plane of rotation, represented by the solid circle.

as for perpendicular transitions (Σ–Π, Π–Σ, etc.), all branches are present.

We define the molecule-fixed z axis to be along $\mathbf{J}$. Thus for Q branch transitions, $\boldsymbol{\mu}$ can be represented as a vector along the z axis. When the transition dipole moment lies in the plane of rotation (P and R transitions), we choose the y axis to lie along $\boldsymbol{\mu}$. Figure 2 shows an illustration of this situation where θ is the angle between the laser polarization vector $\mathbf{E}$ and the rotational angular momentum vector $\mathbf{J}$ of the molecule. The Euler angle χ defines the angle in the plane of rotation which is measured from the line of nodes to the y axis.

It is important to note that we are describing an experimental regime which allows for many nuclear rotations between the time of possible initial alignment of the sample (i.e., preferential directionality of $\mathbf{J}$ following a chemical interaction) and the resonant transition, and again between the resonant transition and the ionization step. This effectively randomizes the angle χ between each transition. We mathematically represent this randomization by an independent integration of the angle χ between each of the two excitation steps.[16]

Using the well-known relationship between the space-fixed and molecule-fixed axes, and integrating over the angle χ, $\langle \boldsymbol{\mu}\cdot\mathbf{E}\rangle^2$ is proportional to

$$\langle(\hat{y}\cdot\hat{Z})^2\rangle_{\rm av} = \frac{1}{2\pi}\int_0^{2\pi} (\sin\theta\cdot\sin\chi)^2\, d\chi = \frac{1}{2}\sin^2\theta \qquad (5)$$

for P and R transitions, and

$$\langle(\hat{z}\cdot\hat{Z})^2\rangle_{\rm av} = \frac{1}{2\pi}\int_0^{2\pi} \cos^2\theta\, d\chi = \cos^2\theta \qquad (6)$$

for Q transitions.

With the integrated intensity $I\Delta t$ expressed in units of energy/cm^2, the k_{01} rate constant is a scaled version of the Einstein B coefficient. Using the relationships of Eqs. (5) and (6), we can write the rate constant for the resonant excitation step as

$$k_{01}(\theta) = \frac{3}{2} C_{01} \frac{S(J_0, J_1)}{(2J_0+1)} \sin^2\theta \qquad (7)$$

for P and R branch members, and

$$k_{01}(\theta) = 3\, C_{01} \frac{S(J_0, J_1)}{(2J_0+1)} \cos^2\theta \qquad (8)$$

for Q branch members. Here $S(J_0, J_1)$ is the rotational line strength normalized to

$$\sum_{J_1} S(J_0, J_1) = (2J_0+1), \qquad (9)$$

and C_{01} contains the wavelength dependence of the resonant transition. We choose to measure integrated peak areas from our spectra and thus C_{01} represents a wavelength averaged proportionality constant,[17] which is on the order of $c^2/(8\pi h\nu^3\,\Delta\nu\,\tau)$, where τ is the vibration-specific lifetime for the resonant step. In the limit where the laser bandwidth is much larger than the homogeneous linewidth of the transition, $\Delta\nu$ can be approximated as the laser bandwidth.

The ionization step can be thought of in a similar manner as the resonant step. However, since the ionization transition connects to a continuum state, and there is no photoelectron energy resolution in the ion detection scheme, the final total angular momentum $\mathbf{J}_2$ remains undetermined. Moreover, the partitioning of $\mathbf{J}_2$ into the orbital, spin, and nuclear rotational components for the ion core as well as the orbital angular momentum and spin components for the departing electron is not known in general. Therefore, for the purposes of measuring total REMPI ion yields, it is unnecessary to decouple the total angular momentum of the ion state into its appropriate components. Instead, we sum over all final total angular momentum states. Thus in theory the θ dependence of the ionization transition need only be specified by its fraction of parallel character (see Appendix B).

For simplicity we use the same P, Q, and R notation as above to indicate a change in total angular momentum for the ionization transition. Classically the branching ratios of P, Q, and R transitions within a parallel or perpendicular electronic transition are as given in Table I. The overall θ dependence of k_{12} is the weighted sum over all possible branches:

$$k_{12}(\theta) = \frac{3}{4}\frac{\sigma}{h\nu}[2\Gamma\sin^2\theta + (1-\Gamma)(1+\cos^2\theta)], \qquad (10)$$

where σ is the cross section for the ionization step, ν is the frequency of the ionizing photon, and Γ is the fraction of parallel character, i.e., the amount of parallel character divided by the sum of parallel and perpendicular character.

TABLE I. The classical values for the ionization branching ratios $S(J_1,J_2)/(2J_1+1)$ are listed as a function of change in total angular momentum (J_2-J_1) and transition character. The values for the case of pure perpendicular character have included the contributions from both projections (± 1) of the transition dipole moment on the internuclear axis.

J_2-J_1	Branch notation	Transition character	
		$\parallel(\mu=0)$	$\perp(\mu=\pm1)$
-1	P	1/2	1/4
0	Q	0	1/2
$+1$	R	1/2	1/4

C. Ground state population and alignment: Classical approach

The complete picture of how to relate REMPI line intensities to ground state populations must allow for the possibility of an initially aligned and orientated ground state. For simplicity, we assume that the ground state exhibits cylindrical symmetry. This allows us to write the directionality for the angular momentum distribution only in terms of the projection of the angular momentum onto the symmetry axis, i.e., in terms of a single angle which we label γ. For systems which do not have cylindrical symmetry, the γ dependence of the angular momentum distribution will exhibit a similar expansion as that within the cylindrical symmetry approximation for a fixed azimuthal orientation of the laser propagation axis relative to the coordinate frame of the aligned system. However the coefficients for the expansion differ in their interpretation.[18]

Because this is a two-photon process, where both transitions are sensitive to the alignment of the rotational angular momentum, the overall REMPI probability for linearly polarized light is sensitive to even moments of the alignment distribution as high as the hexadecapole moment.[19] In cases of strong saturation, REMPI may become very weakly sensitive to even higher moments. However, we will expand the ground state alignment distribution only in terms of monopole $A_0^{(0)}$, quadrupole $A_0^{(2)}$, and hexadecapole $A_0^{(4)}$ moments:

$$N_0(J,\gamma,t=0) = A_0^{(0)} + 2A_0^{(2)}P_2(\cos\gamma) + A_0^{(4)}P_4(\cos\gamma), \tag{11}$$

where

$$P_2(\cos\gamma) = \tfrac{1}{2}(3\cos^2\gamma - 1) \tag{12a}$$

and

$$P_4(\cos\gamma) = \tfrac{1}{8}(35\cos^4\gamma - 30\cos^2\gamma + 3). \tag{12b}$$

The monopole term $A_0^{(0)}$ corresponds to the population in the rotational level J, while the other two terms, $A_0^{(2)}$ and $A_0^{(4)}$, carry independent information about the alignment.

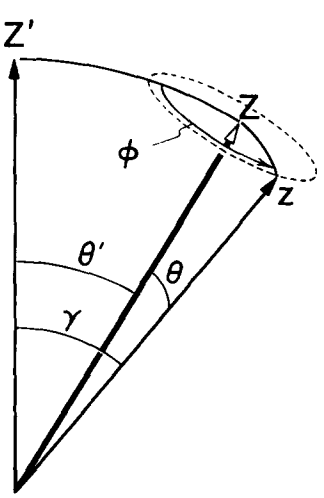

FIG. 3. Relation between the cylindrical symmetry axis which lies along Z', the laser polarization axis which lies along Z, and the rotational angular momentum vector that coincides with z.

The factor of 2 in the quadrupole term is inserted in compliance with the standard notation introduced by Fano and Macek.[20] $A_0^{(2)}$ can span from -1 to $+2$ while $A_0^{(4)}$ spans from $-3/7$ to $+1$.[21]

Although Eq. (11) expresses the alignment distribution in the frame of cylindrical symmetry, the useful coordinate system is that which is defined around the laser polarization axis in the space-fixed frame. Figure 3 illustrates the relationship between the laser polarization axis which lies along Z, the cylindrical symmetry axis which lies along Z', and the molecular axis of rotation which lies along z. The angles are defined as follows: θ' lies between the laser polarization axis Z and the axis of cylindrical symmetry Z', θ lies between the laser polarization axis and the rotational angular momentum vector z, and ϕ is the spherical angle between the arcs of θ and θ'. The relationship between these angles can be expressed as

$$\cos\gamma = \cos\theta\cos\theta' + \sin\theta\sin\theta'\cos\phi. \tag{13}$$

We are interested in the values of $\cos^2\gamma$ and $\cos^4\gamma$ averaged over the rotation ϕ:

$$\langle\cos^2\gamma\rangle_{\rm av} = \frac{1}{2\pi}\int_0^{2\pi}\cos^2\gamma\,d\phi$$

$$= \cos^2\theta\cos^2\theta' + \frac{1}{2}\sin^2\theta\sin^2\theta' \tag{14a}$$

and

$$\langle\cos^4\gamma\rangle_{\rm av} = \frac{1}{2\pi}\int_0^{2\pi}\cos^4\gamma\,d\phi$$

$$= \cos^4\theta\cos^4\theta' + 3\cos^2\theta\cos^2\theta'\sin^2\theta\sin^2\theta'$$

$$+ \frac{3}{8}\sin^4\theta\sin^4\theta'. \tag{14b}$$

In order to write $N_0(J,\theta,\theta',t=0)$ explicitly, the average values of $\cos^2\gamma$ and $\cos^4\gamma$, found in Eqs. (14a) and (14b) can be substituted into Eqs. (12a) and (12b), which in turn are substituted into Eq. (11).

The total ion yield for a REMPI transition from an initially aligned ground state is obtained by substituting into Eq. (2) the explicit expressions for $k_{01}(\theta)$, $k_{12}(\theta)$, and $N_0(J,\theta,\theta',t=0)$ given in Eqs. (7)–(14). The resulting expression is then integrated over all molecular orientations with respect to the polarization vector of the laser beam:

$$N_2(\theta',\Delta t) = \frac{1}{2}\int_0^{\pi} N_0(J,\theta,\theta',t=0)$$

$$\times F_{\rm sat}[k_{01}(\theta),k_{12}(\theta),I\Delta t]\sin\theta\,d\theta. \tag{15}$$

Equation (15), which can be readily evaluated numerically, represents the classical expression for the ion signal intensity in 1 + 1 REMPI. It is seen that the ion yield is a function of the integrated intensity $I\Delta t$ of the laser pulse and θ' (the angle between the axis of cylindrical symmetry and the laser polarization vector). For the special case of no initial alignment in the ground state, Eq. (15) simplifies to

$$N_2(\Delta t) = \frac{1}{2}N_0(J,t=0)$$

$$\times\int_0^{\pi} F_{\rm sat}[k_{01}(\theta),k_{12}(\theta),I\Delta t]\sin\theta\,d\theta. \tag{16}$$

D. REMPI transition rate constants: Quantum mechanical approach

For linearly polarized light the well known $\Delta M = 0$ selection rule applies. In a quantum mechanical approach, we treat the total ionization probability as the sum of probabilities for two independent steps in each M channel: a resonant excitation step and an ionization step.[22] First, we calculate the ground state population and the transition rate constants for each M channel; then we account for saturation using Eqs. (2)–(4).

Within the Born–Oppenheimer framework, a simple wave function can be written to represent a molecular state:

$$|\Psi_{\gamma JM\Omega}\rangle = \Psi_{\text{elec}}\chi_{\text{vib}}\Psi_{\text{rot}}. \tag{17}$$

This describes the electronic, vibrational, and rotational contributions to the overall wave function, where γ represents the electronic quantum numbers, and

$$\Psi_{\text{rot}} = \left[\frac{(2J+1)}{8\pi^2}\right]^{1/2} D^{J}_{M\Omega}(\hat{R})^*. \tag{18}$$

Here, M and Ω correspond to the projections of the total angular momentum $\mathbf{J}$ on the space-fixed laser polarization and molecule fixed internuclear axes, respectively. For the purposes of this calculation we can ignore the parity of the wave function.

The electric dipole approximation for the interaction between the molecule and the semiclassical radiation is of the form

$$\begin{aligned} V &= -\boldsymbol{\mu}\cdot\mathbf{E}(t) \\ &= -(e\Sigma\mathbf{r}_i)\cdot(\mathbf{E}e^{-i\omega t} + \text{c.c.}) \\ &= -(eEe^{-i\omega t} + \text{c.c.})[\Sigma r_i(\hat{\epsilon}\cdot\hat{r}_i)]. \end{aligned} \tag{19}$$

The vector product for polarized light can be written as

$$\begin{aligned} (\hat{\epsilon}\cdot\hat{r}_i) &= \left(\frac{4\pi}{3}\right)^{1/2} Y_{1\mu_0}(\hat{r}_i) \\ &= \left(\frac{4\pi}{3}\right)^{1/2} \sum_{\mu} D^{1}_{\mu_0\mu}(\hat{R})^* Y_{1\mu}(\hat{r}_i). \end{aligned} \tag{20}$$

Here μ_0 corresponds to the polarization of the photon (i.e., $\mu_0 = 0$ or ± 1 for linear or circular polarizations, respectively) while μ is the projection of the photon on the internuclear axis. The Euler angles associated with $\hat{R}$ relate the space-fixed frame to the molecular-fixed frame.

The interaction potential V_{01} is defined as

$$\begin{aligned} V_{01} &= \langle\Psi^{(1)}_{\gamma JM\Omega}|V|\Psi^{(0)}_{\gamma JM\Omega}\rangle \\ &= -\left(\frac{4\pi}{3}\right)^{1/2}(eEe^{-i\omega t} + \text{c.c.})\sum_{\mu}\bar{r}_{01}(\mu) \\ &\quad\times\frac{(2J_1+1)^{1/2}(2J_0+1)^{1/2}}{8\pi^2} \\ &\quad\times\int D^{J_1}_{M_1\Omega_1}(\hat{R})D^{1}_{\mu_0\mu}(\hat{R})^* D^{J_0}_{M_0\Omega_0}(\hat{R})^* d\hat{R}, \end{aligned} \tag{21}$$

where

$$\bar{r}_{01}(\mu) = \int \chi^{(1)}_{\text{vib}}\langle\Psi^{(1)}_{\text{elec}}|\Sigma r_i Y_{1\mu}(\hat{r}_i)|\Psi^{(0)}_{\text{elec}}\rangle\chi^{(0)}_{\text{vib}}\, dR, \tag{22}$$

and R is the internuclear distance. The interaction potential must be integrated over all possible orientations $\hat{R}$ and averaged over time:

$$\begin{aligned} V_{01} &= -eE\left(\frac{4\pi}{3}\right)^{1/2}(2J_1+1)^{1/2}(2J_0+1)^{1/2} \\ &\quad\times\sum_{\mu}(-1)^{M_0+\mu_0-\Omega_0-\mu}\bar{r}_{01}(\mu) \\ &\quad\times\begin{pmatrix} J_1 & 1 & J_0 \\ \Omega_1 & -\mu & -\Omega_0 \end{pmatrix}\begin{pmatrix} J_1 & 1 & J_0 \\ M_1 & -\mu_0 & -M_0 \end{pmatrix}. \end{aligned} \tag{23}$$

The rate constant k_{01} is proportional to the square of the interaction potential V_{01}. With the restriction of linearly polarized light, the following substitutions are made: $\mu_0 = 0$ and $M = M_0 = M_1$. For intermediate coupling cases where Ω is not a good quantum number, the exact wave function can be represented as an expansion of the aforementioned complete basis set. This is accounted for in the rotational line strength factors of the resonant transition. Hence the equation for $k_{01}(M)$ becomes

$$k_{01}(M) = 3\,C_{01}\,S(J_0,J_1)\begin{pmatrix} J_1 & 1 & J_0 \\ M & 0 & -M \end{pmatrix}^2, \tag{24}$$

where C_{01} is a proportionality constant whose value has been discussed in Sec. II B.

In a similar manner the interaction potential for the ionization transition can be calculated. We will choose to represent the intermediate state as a Hund's case (b) wave function:

$$\begin{aligned} \Psi_{J_1,N_1,S,\Lambda_1,M} &= \left[\frac{(2J_1+1)(2N_1+1)}{8\pi^2}\right]^{1/2}(-1)^{S-N_1-M} \\ &\quad\times\sum_{M_S}\begin{pmatrix} N_1 & S & J_1 \\ M-M_S & M_S & -M \end{pmatrix} \\ &\quad\times D^{N_1}_{M-M_S,\Lambda_1}(\hat{R})^*\,|SM_s\rangle. \end{aligned} \tag{25}$$

Here, $\mathbf{N}_1$ is the angular momentum due to nuclear rotation, $\mathbf{J}_1$ is the total angular momentum excluding nuclear spin, $\mathbf{S}$ is the total electron spin for the system (which is conserved throughout), M and M_S are the projections of $\mathbf{J}_1$ and $\mathbf{S}$, respectively, on the space-fixed frame, and Λ_1 is the projection of $\mathbf{N}_1$ on the internuclear axis. The final ion state can be represented by any complete basis set, since we will sum over all basis set numbers in the final analysis:

$$\Psi_{N_2,S,M,M_S} = \left[\frac{(2N_2+1)}{8\pi^2}\right]^{1/2} D^{N_2}_{M\Lambda_2}(\hat{R})^*\,|SM_s\rangle. \tag{26}$$

Here $\mathbf{N}_2$ is the coupled angular momentum of nuclear rotation and electronic orbital angular momentum for both the ion core and the departing electron and Λ_2 is the projection of $\mathbf{N}_2$ on the internuclear axis.

The interaction potential V_{12} can be written as

$$V_{12} = -eE\left(\frac{4\pi}{3}\right)^{1/2}(2N_1+1)^{1/2}(2J_1+1)^{1/2}(2J_2+1)^{1/2}(-1)^{N_1-\Lambda_1}\sum_{M_S\mu\Lambda_2}(-1)^{S-\mu-M_S}$$
$$\times\begin{pmatrix} N_1 & S & J_1 \\ M-M_S & M_S & -M\end{pmatrix}\begin{pmatrix} N_2 & 1 & N_1 \\ M-M_S & 0 & M_S-M\end{pmatrix}\begin{pmatrix} N_2 & 1 & N_1 \\ \Lambda_2 & -\mu & -\Lambda_1\end{pmatrix}\bar{r}_{12}(\mu). \tag{27}$$

We are interested in the square of the interaction potential summed over all final states:

$$V_{12}^2 = \sum_{M_S}(2J_1+1)\begin{pmatrix} N_1 & S & J_1 \\ M-M_S & M_S & -M\end{pmatrix}^2\sum_{N_2\mu\Lambda_2}e^2E^2\left(\frac{4\pi}{3}\right)(2N_1+1)(2N_2+1)\bar{r}_{12}^2(\mu)$$
$$\times\begin{pmatrix} N_2 & 1 & N_1 \\ M-M_S & 0 & M_S-M\end{pmatrix}^2\begin{pmatrix} N_2 & 1 & N_1 \\ \Lambda_2 & -\mu & -\Lambda_1\end{pmatrix}^2. \tag{28}$$

When measuring total ions from a REMPI process in which the ion state is not detected, one sums incoherently over μ, the projection of the photon angular momentum on the internuclear axis (see Appendix B). The rate constant k_{12} is proportional to V_{12}^2 of Eq. (28). For simplicity we will define σ to be the overall cross section, Γ to be the fraction of parallel character, and Δ to be the difference between the $\mu = \pm 1$ channels, such that the partial cross sections can be written as

$$\sigma(\mu=0) = \sigma\Gamma, \tag{29a}$$
$$\sigma(\mu=+1) = \sigma\tfrac{1}{2}(1-\Gamma+\Delta), \tag{29b}$$

and

$$\sigma(\mu=-1) = \sigma\tfrac{1}{2}(1-\Gamma-\Delta). \tag{29c}$$

Here, Γ spans from 0 to 1 and Δ from $-(1-\Gamma)$ to $(1-\Gamma)$. The parameter Δ is exactly 0 for ionization out of a intermediate state having Σ symmetry. With these substitutions the expression for $k_{12}(M)$ [for the case (b) coupling scheme] becomes

$$k_{12}(M) = 3(2N_1+1)(2J_1+1)\frac{\sigma}{h\nu}\sum_{M_S}\begin{pmatrix} N_1 & S & J_1 \\ M-M_S & M_S & -M\end{pmatrix}^2\sum_{N_2}(2N_2+1)\begin{pmatrix} N_2 & 1 & N_1 \\ M-M_S & 0 & M_S-M\end{pmatrix}^2$$
$$\times\left[\Gamma\begin{pmatrix} N_2 & 1 & N_1 \\ \Lambda_1 & 0 & -\Lambda_1\end{pmatrix}^2+\frac{1}{2}(1-\Gamma+\Delta)\begin{pmatrix} N_2 & 1 & N_1 \\ \Lambda_1+1 & -1 & -\Lambda_1\end{pmatrix}^2\right.$$
$$\left.+\frac{1}{2}(1-\Gamma-\Delta)\begin{pmatrix} N_2 & 1 & N_1 \\ \Lambda_1-1 & 1 & -\Lambda_1\end{pmatrix}^2\right]. \tag{30}$$

Only two sums are required, i.e., M_S and N_2 span between $-S$ and $+S$, and $|N_1-1|$ and N_1+1, respectively. Note that the $k_{12}(M)$ distribution is insensitive to the parameter Δ in the high J limit, and Eq. (30) approaches the form of Eq. (10).

The equivalent expression to Eq. (30) for photoionization from an intermediate state having pure case (a) coupling is

$$K_{12}(M) = 3(2J_1+1)\frac{\sigma}{h\nu}\sum_{J_2}(2J_2+1)\begin{pmatrix} J_2 & 1 & J_1 \\ M & 0 & -M\end{pmatrix}^2$$
$$\times\left[\Gamma\begin{pmatrix} J_2 & 1 & J_1 \\ \Omega_1 & 0 & -\Omega_1\end{pmatrix}^2+\frac{1}{2}(1-\Gamma+\Delta)\right.$$
$$\times\begin{pmatrix} J_2 & 1 & J_1 \\ \Omega_1+1 & -1 & -\Omega_1\end{pmatrix}^2$$
$$\left.+\frac{1}{2}(1-\Gamma-\Delta)\begin{pmatrix} J_2 & 1 & J_1 \\ \Omega_1-1 & 1 & -\Omega_1\end{pmatrix}^2\right], \tag{31}$$

where Ω is the projection of J on the internuclear axis.

Figure 4 shows the M-dependent transition rate constants in their limiting cases: the resonant transition is characterized by either P, R, or Q branch notation; and the ionization transition is shown for the limiting cases of pure parallel or perpendicular character.

The parameters, σ and Γ (and Δ for low J transitions),

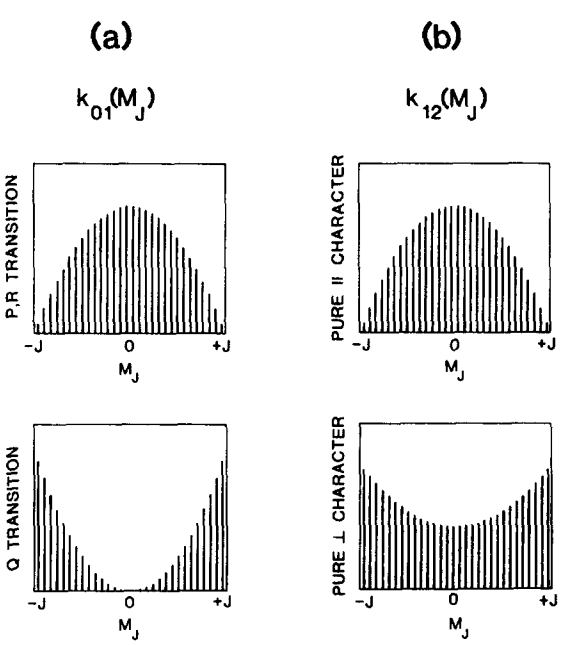

FIG. 4. The M-dependent rate constants are shown for transitions originating from the $J = 14.5$ rotational level of the ground state. In (a) the resonant rate constant $k_{01}(M)$ is shown for the two different branch types (P–R and Q), while in (b) the ionization rate constant $k_{12}(M)$ is illustrated for the two limiting cases of pure parallel and pure perpendicular character.

are sometimes estimated through *ab initio* calculations or determined experimentally. Excited state lifetimes for most resonant transitions have been measured; however, ionization transitions are more illusive. In the common limit where $k_{12} \ll k_{01}$ the 1 + 1 REMPI relative ion yields are more dependent on the fraction of parallel character than they are on the absolute magnitude of the ionization cross section. This is because the fraction of parallel character predicts the shape of the $k_{12}(M)$ distribution, while, in the limit where $k_{12} \ll k_{01}$, the magnitude of the overall ionization cross section only slightly changes the depletion rate of the intermediate state population and thus has little effect on the degree of saturation.

E. Ground state population and alignment: Quantum mechanical approach

Similar to the classical model for ground state alignment, we expand the ground state M' population distribution in terms of monopole $A_0^{(0)}$, quadrupole $A_0^{(2)}$, and hexadecapole $A_0^{(4)}$ terms as defined in the primed cylindrically symmetric frame. This can be expressed as an operator $\mathbf{N}_0'$:

$$\mathbf{N}_0' = A_0^{(0)} + 2A_0^{(2)}\left[\frac{3\mathbf{J}_z'^2 - \mathbf{J}^2}{2\mathbf{J}^2}\right] + A_0^{(4)}\left[\frac{3\mathbf{J}^4 - 6\mathbf{J}^2 - 30\mathbf{J}^2\mathbf{J}_z'^2 + 25\mathbf{J}_z'^2 + 35\mathbf{J}_z'^4}{8\mathbf{J}^4}\right]. \tag{32}$$

Note that Eq. (32) is the quantum mechanical analog of Eq. (11). The population in state $|J,M'\rangle$ is equivalent to the expectation value of the operator $\mathbf{N}_0'$ in the state $|J,M'\rangle$:

$$N_0(J,M',t=0) = \langle J,M'|\mathbf{N}_0'|J,M'\rangle. \tag{33}$$

Assume the laser polarization axis Z makes an arbitrary angle, characterized by the Euler angles (ϕ',θ',χ'), to the axis of cylindrical symmetry Z'. The laser acts on the molecules in accordance with their quantization in the laser frame. The eigenvectors in the laser frame are related to those in the cylindrical symmetry frame through a rotational transformation[23]:

$$\mathscr{R}(\phi',\theta',\chi')|J,M\rangle = \sum_{M'} D^J_{M',M}(\phi',\theta',\chi')|J,M'\rangle. \tag{34}$$

The population in state $|J,M\rangle$ of the rotated laser frame is equivalent to the expectation value of the operator $\mathbf{N}_0$ on the state $|J,M\rangle$. Thus

$$N_0(J,M,\theta',t=0) = \langle J,M|\mathbf{N}_0'|J,M\rangle = \sum_{M'} |d^J_{M',M}(\theta')|^2\langle J,M'|\mathbf{N}_0'|J,M'\rangle. \tag{35}$$

Substitution of Eq. (32) into Eq. (35) gives

$$N_0(J,M,\theta',t=0) = A_0^{(0)} + A_0^{(2)}\left[-1 + \frac{3}{J(J+1)}\sum_{M'}|d^J_{M',M}(\theta')|^2 M'^2\right] + A_0^{(4)}\left\{\frac{3}{8} - \frac{3}{4J(J+1)} - \frac{5}{8J^2(J+1)^2}\sum_{M'}|d^J_{M',M}(\theta')|^2\left[6J(J+1)M'^2 + 5M'^2 + 7M'^4\right]\right\}, \tag{36}$$

where we have used the identity

$$\sum_{M'}|d^J_{M',M}(\theta')|^2 = 1. \tag{37}$$

Having calculated the M-dependent ground state populations $N_0(J,M,\theta',t=0)$ [Eq. (36)], and rate constants $k_{01}(M)$ and $k_{12}(M)$ [Eqs. (24) and (30)], we can solve the saturation equation [Eq. (2)] for each individual M channel. The total ion yield is just the sum over the ion yields resulting from each M channel:

$$N_2(\theta',\Delta t) = \sum_M N_0(J,M,\theta',t=0)F_{\text{sat}}[k_{01}(M),k_{12}(M),I\Delta t]. \tag{38}$$

For a system having no initial alignment in the ground state, the total ion yield becomes

$$N_2(\Delta t) = N(J,t=0)\sum_M F_{\text{sat}}[k_{01}(M),k_{12}(M),I\Delta t]. \tag{39}$$

F. Loss of ground state alignment information

It is worthwhile at this point to mention some of the limitations in measuring ground state alignment. As has been outlined in this paper, saturation does indeed have an effect on the overall M-dependent transition rates. Higher laser powers will in general destroy the overall amount of alignment information that can be obtained, because the effective $k_{01}(M)$ distribution flattens out with saturation. This is demonstrated elsewhere.[10] Two other effects that actually randomize ground state alignment are hyperfine depolarization and magnetic precession.

Hyperfine depolarization only applies to systems with nonzero nuclear spin **I**, for which the hyperfine structure is spectrally unresolved. It is due to the precession of **J** about the true quantum vector **F**, since only total angular momentum is conserved. The precession frequency is on the order of the hyperfine splitting. If this precession is fast relative to the time difference between initial alignment and absorption, then the ground state magnetic sublevel distribution will be somewhat scrambled. The fraction of alignment information

remaining in the k th moment of the ground state distribution has been shown to be[20,24]

$$\bar{g}^{(k)} = \sum_i \frac{(2F_i+1)^2}{(2I+1)} \begin{Bmatrix} F_i & F_i & k \\ J & J & I \end{Bmatrix}^2. \tag{40}$$

For $J \gg I$ the effect is negligible, and $\bar{g}^{(k)}$ approaches unity. Only for cases of very strong hyperfine coupling in the intermediate state, where the period of precession is fast compared to the laser pulse width, will the intermediate state also be scrambled.

Magnetic precession occurs in the presence of an external magnetic field (the Earth's field, fields from heater filaments, etc.) with molecules having a permanent magnetic moment. The magnetic field defines the quantization axis about which the molecule will precess. The precession frequency is defined to be

$$f = (8.8\ \text{MHz/G})\ \frac{(\Lambda+2\Sigma)(\Lambda+\Sigma)M}{J(J+1)} H \tag{41a}$$

for Hund's case (a), and

$$f = (8.8\ \text{MHz/G}) \left[\frac{\Lambda^2 M_K}{K(K+1)} + 2M_s\right] H \tag{41b}$$

for Hund's case (b), where H is the magnetic field strength and M is defined as the projection of angular momentum along the magnetic field axis.[25]

If the period of precession for the intermediate state is far less than the duration of the laser pulse, then quantum beats or coherences between the resonant transition and ionization are not of concern. However if the period of precession for the ground state is much greater than the time between initial alignment and absorption, then the polarization information obtained by REMPI will be altered in the following manner:

Let us define the angle between the cylindrical symmetry axis and the magnetic field direction as θ'' and redefine the angle θ' to be the angle between the magnetic field vector and the plane of polarization. Then in a quantum mechanical derivation similar to that of Eq. (35), we find

$$N_0(J,M,\theta',\theta'',t=0) = \sum_{M''} |d^J_{M'',M}(\theta')|^2 \sum_{M'} |d^J_{M',M''}(\theta'')|^2 N_0(J,M'). \tag{42}$$

Equation (42) can be expanded as

$$\begin{aligned} N_0(J,M,\theta',\theta'',t=0) = {} & A_0^{(0)} + A_0^{(2)}\bar{g}^{(2)} \left[-1 + \frac{3}{J(J+1)} \sum_{M''} \sum_{M'} |d^J_{M'',M}(\theta') d^J_{M',M''}(\theta'')|^2 M'^2 \right] \\ & + A_0^{(4)}\bar{g}^{(4)} \left\{ \frac{3}{8} - \frac{3}{4J(J+1)} - \frac{5}{8J^2(J+1)^2} \right. \\ & \left. \times \sum_{M''} \sum_{M'} |d^J_{M'',M}(\theta') d^J_{M',M''}(\theta'')|^2 [6J(J+1)M'^2 + 5M'^2 + 7M'^4] \right\}. \end{aligned} \tag{43}$$

Note that in the special cases where the magnetic field vector points in the same direction as the axis of cylindrical symmetry ($\theta'' = 0$), or the magnetic field coincides with the laser polarization axis ($\theta' = 0$), then no magnetic field depolarization effect will be observed.

The classical mechanical equivalent to Eq. (43) can be found through double substitution of Eqs. (14a) and (14b), to yield the results

$$\langle \cos^2 \gamma \rangle_{\text{av}} = (\cos^2\theta \cos^2\theta' + \sin^2\theta \sin^2\theta')(\cos^2\theta'' - \tfrac{1}{2}\sin^2\theta'') + \tfrac{1}{2}\sin^2\theta'', \tag{44a}$$

and

$$\begin{aligned} \langle \cos^4 \gamma \rangle_{\text{av}} = {} & -\tfrac{3}{8}\sin^4\theta'' + (\tfrac{3}{8}\sin^4\theta'' + \cos^4\theta'') \\ & \times (\cos^4\theta\cos^4\theta' + 3\cos^2\theta\cos^2\theta'\sin^2\theta\sin^2\theta' + \tfrac{3}{8}\sin^4\theta\sin^4\theta') \\ & + 3\sin^2\theta''(1 - \cos^2\theta\cos^2\theta' - \tfrac{1}{2}\sin^2\theta\sin^2\theta') \\ & \times [\tfrac{1}{4}\sin^2\theta'' + \cos^2\theta''(\cos^2\theta\cos^2\theta' + \tfrac{1}{2}\sin^2\theta\sin^2\theta')]. \end{aligned} \tag{44b}$$

In order to write $N_0(J,\theta,\theta',\theta'',t=0)$ explicitly, Eqs. (44a) and (44b) are substituted into Eqs. (12a) and (12b) which in turn are substituted into Eq. (11). Equation (11) defines the population of the probed system for molecules having angular momentum vectors at an angle θ to the laser polarization axis.

III. COMPARISON OF CLASSICAL AND QUANTUM MECHANICAL APPROACHES

This paper has derived mathematical expressions to relate 1 + 1 REMPI ion intensities to ground state populations and alignment factors, through the inclusion of the interdependent effects of saturation and intermediate state alignment. Both classical and quantum mechanical treatments were pursued. It is useful at this point to comment on the appropriate regimes for these approaches.

Let us choose a theoretical system in order to make an appropriate comparison. One commonly encountered REMPI system is that of a one-photon $^1\Pi$–$^1\Sigma$ resonant transition followed by a one-photon ionization transition. Let us assume that $k_{01} \gg k_{12}$ and indicate the degree of resonant saturation by the dimensionless product $k_{01} I \Delta t$.[26] Calcula-

tions were performed on all resonant transition branches and both limiting cases of parallel and perpendicular character for the ionization transition. The comparisons reported below represent the worst case out of the permutations of the preceding limiting cases. For cases where the saturation product $k_{01}I\Delta t$ was as high as 10, we found that the classical predictions for the ion yield agreed with those from the quantum calculation to within 5% for $J_0 > 2$. The calculations for the polarization dependence of an aligned distribution were found to differ by less than 5% for $J_0 > 4$. One finds other problems that often plague low J regimes, such as hyperfine depolarization, that minimize the amount of alignment information to be gained in any case. For most molecular (but not atomic) systems, J_0 exceeds four. Therefore we conclude that the simpler classical approach suffices for calculating $1+1$ REMPI ion yields in almost all molecular cases of interest.

ACKNOWLEDGMENTS

D. C. J. wishes to thank R. J. Madix for his patient support, S. Dixit for helpful conversations and preprints, and A. Kummel for useful discussions. This work was supported by Amoco.

APPENDIX A: DEPENDENCE OF ION YIELD ON PULSE CHARACTERISTICS

Using a three-level rate model, Sec. II A derived an expression [Eq. (2)] for the ion yield $N_2(\Delta t)$ resulting from a rectangular pulse of intensity I and duration Δt. The assumption of a rectangular pulse shape makes the solution of the three coupled differential equations of this model [Eqs. (1a)–(1c)] readily tractable. However this form is a poor approximation to realistic pulse shapes. Nevertheless, we show here that the important parameter in determining the value of $N_2(\Delta t)$ is not the shape of the pulse but its integrated intensity (fluence), which for a rectangular pulse shape is simply $I\Delta t$. Moreover pulses having different shapes but the same integrated intensity produce approximately the same ion yields.

The rate equations shown in Eqs. (1a)–(1c) may be written in the form

$$\frac{dN_j(t)}{dt} = I(t)F_j(t), \tag{A1}$$

where $j = 1$, 2, or 3, and the function $F_j(t)$ does not depend explicitly on the instantaneous intensity. It follows that $N_j(t+\delta t)$ is related to $N_j(t)$ by

$$N_j(t+\delta t) = N_j(t) + I(t+\delta t)F_j(t)\delta t, \tag{A2}$$

where δt is a small increment of time. It is useful to regard an arbitrary pulse of instantaneous intensity $I(t)$ and duration τ as composed of a succession of N rectangular pulses in which the ith pulse has a height $I(i\tau/N)$ and a width $\delta t = \tau/N$. In the limit as N becomes large, this approximation becomes exact for physically reasonable pulse shapes. The index i runs from 1 to N and the integrated intensity is approximately given by

$$\int_0^\tau I(t)dt \simeq \sum_{i=1}^{N} I(i\tau/N)(\tau/N). \tag{A3}$$

According to Eq. (A2) the population in level j after the ith pulse is given by

$$N_j[(i+1)\tau/N] = N_j(i\tau/N) + I[(i+1)\tau/N]F_j(i\tau/N)(\tau/N), \tag{A4}$$

where we replaced the time increment δt by τ/N. Hence each successive rectangular pulse adds to the previous sum a quantity:

$$\Delta N_j = I[(i+1)\tau/N]F_j(i\tau/N)(\tau/N). \tag{A5}$$

Suppose the arbitrary pulse is rescaled so that its instantaneous intensity is multiplied by the factor c while its duration is divided by the factor c. Reference to Eq. (A3) shows that such a pulse has the same integrated intensity, and we refer to such a pulse as having the same pulse form as the unscaled pulse. For this pulse Eq. (A5) becomes

$$\Delta N_j' = cI[(i+1)c\tau'/N]F_j'(i\tau'/N)(\tau/cN) = I[(i+1)\tau/N]F_j'(i\tau'/N)(\tau/N), \tag{A6}$$

where the increments of time are c times smaller than the unscaled pulse (i.e., $\tau'/N = \tau/cN$). We conclude that $\Delta N_j'$ is equivalent to ΔN_j provided that $F_j'(i\tau'/N)$ for the scaled pulse is equivalent to $F_j(i\tau/N)$ for the original pulse. But the function F_j depends only on the rate constants and the instantaneous populations of the three levels. Under the same initial conditions, the population after the first rectangular pulse of the pulse train will be the same for both pulses. As successive pulses act on the system, the population will be changed by the same amount for both pulse profiles at each value of the index i. Therefore the final ion yield, $N_2(\tau)$, is the same for all pulses having the same pulse form and same integrated intensity.

Next we consider the ion yield resulting from two pulses having the same integrated intensity but different pulse forms. We compare numerically the value of $N_2(\tau)$ resulting from a Gaussian pulse with that from a rectangular pulse having the same integrated intensity $I\Delta t$. We take $k_{01} \gg k_{12}$, as is commonly the case. Even in saturation regimes where $k_{01}I\Delta t = 4$ or 10, we find that the ion yields resulting from the two different pulse shapes with the same integrated intensity differ by less than 5% and 10%, respectively. Thus for much practical work in $1+1$ REMPI, it appears justified to replace the actual pulse shape by a rectangular pulse having the same integrated intensity. This is an important simplification because in many laser systems the detailed pulse form varies from shot to shot.

APPENDIX B: CONNECTION WITH ANGULAR MOMENTUM TRANSFER FORMALISM

In the photoionization step the photoelectron is conveniently described as an expansion in terms of partial waves. This description allows for interference between the indistinguishable pathways of ionization leading to a given ion state. These interference terms are well known and account for the form of the photoelectron angular distribution. However, we desire to find an expression for the total ion yield when the molecular ion final state as well as the photoelectron energy and angular distribution are not measured. We show that

interference terms between the continuum channels do not change the expression for $k_{12}(M)$ given by Eq. (30), i.e., the $k_{12}(M)$ distribution can be completely described in terms of the parallel ($\Delta\Lambda = 0$) and perpendicular ($\Delta\Lambda = \pm 1$) characters of the bound-to-free transition.

Our starting point is the expression adapted from Eq. (14) of Dixit and McKoy[22] for the matrix element of the interaction Hamiltonian written in terms of the angular momentum transfer formalism. Other authors have derived similar equations for the matrix element[27–29]:

$$V_{12} = -eE\left(\frac{4\pi}{3}\right)^{1/2} \sum_{lm\lambda\mu} \sum_{j_t m_t \lambda_t} (2j_t+1)(-i)^l e^{i\eta} Y_{lm}(\hat{k})(-1)^{\mu-\mu_0+M_+-\Lambda_++m_t-\lambda_t}$$
$$\times (2N_1+1)^{1/2}(2N_++1)^{1/2}\bar{r}_l(\mu)\begin{pmatrix} N_+ & N_1 & j_t \\ -M_+ & M_1 & m_t\end{pmatrix}\begin{pmatrix} N_+ & N_1 & j_t \\ -\Lambda_+ & \Lambda_1 & \lambda_t\end{pmatrix}$$
$$\times\begin{pmatrix} l & 1 & j_t \\ -m & \mu_0 & -m_t\end{pmatrix}\begin{pmatrix} l & 1 & j_t \\ -\lambda & \mu & -\lambda_t\end{pmatrix}. \tag{B1}$$

Here $\mathbf{j}_t$ is the angular momentum transferred to the molecular ion with projections m_t and λ_t on the laboratory and molecule-fixed z axes, $\mathbf{N}_+$ is the angular momentum of the molecular ion with projections M_+ and Λ_+, $\mathbf{N}_1$ is the angular momentum of the intermediate state with projections M_1 and Λ_1, the dipole photon has unit angular momentum with projections μ_0 and μ, and $\mathbf{l}$ is the orbital angular momentum of the photoelectron in partial wave l with projections m and λ. The phase shift η depends on l and λ and the photoelectron has a momentum $|\mathbf{k}|$ and a direction $\hat{\mathbf{k}}$. In Eq. (B1), $\bar{r}_l(\mu)$ is the radial integral of the electric dipole moment. It is integrated over electron coordinates and internuclear distance. The bound–free rate constant $k_{12}(M)$ is proportional to the square of V_{12} integrated over the photoelectron energy and angular distribution. In what follows we show that when we square and integrate V_{12} in Eq. (B1) the resulting expression can be put into a form similar to Eq. (28).

We concentrate on the product of the four 3-j symbols appearing in Eq. (B1). We introduce the identities:

$$\begin{pmatrix} l & 1 & j_t \\ -m & \mu_0 & -m_t\end{pmatrix}\begin{pmatrix} l & 1 & j_t \\ -\lambda & \mu & -\lambda_t\end{pmatrix} = (8\pi^2)^{-1}\int D^{l}_{-m-\lambda}(\hat{R})D^{1}_{\mu_0\mu}(\hat{R})D^{j_t}_{-m_t-\lambda_t}(\hat{R})d\hat{R}, \tag{B2}$$

$$\sum_{j_t m_t \lambda_t}(2j_t+1)\begin{pmatrix} N_+ & N_1 & j_t \\ -M_+ & M_1 & m_t\end{pmatrix}\begin{pmatrix} N_+ & N_1 & j_t \\ -\Lambda_+ & \Lambda_1 & \lambda_t\end{pmatrix}D^{j_t}_{m_t\lambda_t}(\hat{R})^* = D^{N_+}_{-M_+-\Lambda_+}(\hat{R})D^{N_1}_{M_1\Lambda_1}(\hat{R}), \tag{B3}$$

and

$$D^{j_t}_{m_t\lambda_t}(\hat{R})^* = (-1)^{m_t-\lambda_t}D^{j_t}_{-m_t-\lambda_t}(\hat{R}). \tag{B4}$$

Substitution of these into Eq. (B1) gives

$$V_{12} = -eE\left(\frac{4\pi}{3}\right)^{1/2}\sum_{lm\lambda\mu}(-i)^l e^{i\eta}Y_{lm}(\hat{k})(-1)^{\mu-\mu_0+M_+-\Lambda_+}$$
$$\times(2N_1+1)^{1/2}(2N_++1)^{1/2}\bar{r}_l(\mu)(8\pi^2)^{-1}\int D^{l}_{-m-\lambda}(\hat{R})D^{1}_{\mu_0\mu}(\hat{R})D^{N_+}_{-M_+-\Lambda_+}(\hat{R})D^{N_1}_{M_1\Lambda_1}(\hat{R})d\hat{R}. \tag{B5}$$

We recouple the photoelectron orbital angular momentum $\mathbf{l}$ with the molecular ion angular momentum $\mathbf{N}_+$ to form the resultant $\mathbf{N}_2$. Using similar identities to reverse our steps we find that

$$V_{12} = -eE\left(\frac{4\pi}{3}\right)^{1/2}\sum_{lm\lambda\mu}\sum_{N_2M_2\Lambda_2}(2N_2+1)(-i)^l e^{i\eta}Y_{lm}(\hat{k})(-1)^{\mu-\mu_0+M_+-\Lambda_++M_2-\Lambda_2}$$
$$\times(2N_1+1)^{1/2}(2N_++1)^{1/2}\bar{r}_l(\mu)\begin{pmatrix} N_+ & l & N_2 \\ -M_+ & -m & M_2\end{pmatrix}\begin{pmatrix} N_+ & l & N_2 \\ -\Lambda_+ & -\lambda & \Lambda_2\end{pmatrix}$$
$$\times\begin{pmatrix} N_1 & 1 & N_2 \\ M_1 & \mu_0 & -M_2\end{pmatrix}\begin{pmatrix} N_1 & 1 & N_2 \\ \Lambda_1 & \mu & -\Lambda_2\end{pmatrix}. \tag{B6}$$

Note the similarity to Eq. (B1), where N_2 takes the place of j_t. We regroup this expression into the product of two terms:

$$\mathbf{V}_{12} = \sum_{lm\lambda\mu}\sum_{N_2M_2\Lambda_2}(-i)^l e^{i\eta}Y_{lm}(\hat{k})(2N_++1)^{1/2}(2N_2+1)^{1/2}(-1)^{M_2-\Lambda_2}$$
$$\times\begin{pmatrix} N_+ & l & N_2 \\ -M_+ & -m & M_2\end{pmatrix}\begin{pmatrix} N_+ & l & N_2 \\ -\Lambda_+ & -\lambda & \Lambda_2\end{pmatrix}$$
$$\times\left[-eE\left(\frac{4\pi}{3}\right)^{1/2}(2N_1+1)^{1/2}(2N_2+1)^{1/2}(-1)^{\mu-\mu_0+M_2-\Lambda_2}\bar{r}_l(\mu)\right.$$
$$\left.\times\begin{pmatrix} N_2 & 1 & N_1 \\ M_2 & -\mu_0 & -M_1\end{pmatrix}\begin{pmatrix} N_2 & 1 & N_1 \\ \Lambda_2 & -\mu & -\Lambda_1\end{pmatrix}\right]. \tag{B7}$$

We now choose to square Eq. (B7) and integrate over all spatial directions of the emitted photoelectron. Note that the orthonormality of the spherical harmonics creates an incoherent sum over l and m:

$$\int V_{12}^2(\hat{k})d\hat{k} = \sum_{lm}(2N_+ + 1)\left\{\sum_{N_2\Lambda_2\mu\lambda} e^{i\eta}(2N_2+1)^{1/2} \times\begin{pmatrix} N_+ & l & N_2 \\ -M_+ & -m & M_2\end{pmatrix}\begin{pmatrix} N_+ & l & N_2 \\ -\Lambda_+ & -\lambda & \Lambda_2\end{pmatrix} \times\left[-eE\left(\frac{4\pi}{3}\right)^{1/2}(2N_1+1)^{1/2}(2N_2+1)^{1/2}(-1)^{\mu-\mu_0+M_2-\Lambda_2}\bar{r}_l(\mu) \times\begin{pmatrix} N_2 & 1 & N_1 \\ M_2 & -\mu_0 & -M_1\end{pmatrix}\begin{pmatrix} N_2 & 1 & N_1 \\ \Lambda_2 & -\mu & -\Lambda_1\end{pmatrix}\right]\right\}^2. \tag{B8}$$

We utilize the identity:

$$\sum_m\left[\sum_{N_2}(2N_2+1)^{1/2}f(N_2)\begin{pmatrix} N_+ & l & N_2 \\ m-M_2 & -m & M_2\end{pmatrix}\right]^2 = \sum_{N_2} f(N_2)^2. \tag{B9}$$

Insertion of this into Eq. (B8) gives

$$\int V_{12}^2(\hat{k})d\hat{k} = \sum_{N_2lm}(2N_+ + 1)\left\{\sum_{\Lambda_2\mu\lambda} e^{i\eta}\begin{pmatrix} N_+ & l & N_2 \\ -\Lambda_+ & -\lambda & \Lambda_2\end{pmatrix} \times\left[-eE\left(\frac{4\pi}{3}\right)^{1/2}(2N_1+1)^{1/2}(2N_2+1)^{1/2}(-1)^{\mu-\mu_0+M_2-\Lambda_2}\bar{r}_l(\mu) \times\begin{pmatrix} N_2 & 1 & N_1 \\ M_2 & -\mu_0 & -M_1\end{pmatrix}\begin{pmatrix} N_2 & 1 & N_1 \\ \Lambda_2 & -\mu & -\Lambda_1\end{pmatrix}\right]\right\}^2. \tag{B10}$$

Additionally we must sum over all possible ion state quantum numbers (N_+ and M_+). The sum over N_+ occurs incoherently because photoelectrons emitted from ions having different N_+ will have different energies and thus cannot interfere. We utilize another 3-j symbol orthogonality:

$$\sum_{N_+}\left[(2N_+ + 1)\sum_{\lambda\Lambda_2} f(\lambda,\Lambda_2)\begin{pmatrix} N_+ & l & N_2 \\ -\Lambda_+ & -\lambda & \Lambda_2\end{pmatrix}\right]^2 = \sum_{\lambda\Lambda_2} f(\lambda,\Lambda_2)^2. \tag{B11}$$

We then arrive at

$$\int V_{12}^2(\hat{k})d\hat{k} = \sum_{N_2\mu\Lambda_2} e^2E^2\left(\frac{4\pi}{3}\right)(2N_1+1)(2N_2+1)\bar{r}_{12}^2(\mu) \times\begin{pmatrix} N_2 & 1 & N_1 \\ M_2 & -\mu_0 & -M_1\end{pmatrix}^2\begin{pmatrix} N_2 & 1 & N_1 \\ \Lambda_2 & -\mu & -\Lambda_1\end{pmatrix}^2, \tag{B12}$$

where we have defined $\bar{r}_{12}^2(\mu)$ to be the following:

$$\bar{r}_{12}^2(\mu) \equiv \sum_l \bar{r}_l^2(\mu). \tag{B13}$$

Equation (B12) is seen to be similar to Eq. (28) in this paper. Note that the sum over μ, the projection of the photon angular momentum on the internuclear axis, is incoherent. Therefore the $k_{12}(M)$ distribution need only be specified by at most three parameters: σ, Γ, and Δ.

[1] D. H. Parker, in *Ultrasensitive Laser Techniques*, edited by D. S. Klieger (Academic, New York, 1983), see references therein.
[2] D. L. Feldman, R. K. Lengel, and R. N. Zare, Chem. Phys. Lett. **52**, 413 (1977).
[3] L. Bigio and E. R. Grant, J. Phys. Chem. **89**, 5855 (1985).
[4] E. E. Marinero, C. T. Rettner, and R. N. Zare, J. Chem. Phys. **80**, 4142 (1984).
[5] D. S. King and R. R. Cavanagh, *Laser Surface Studies* (Springer, Berlin, 1984), see references therein.
[6] G. D. Kubiak, G. O. Sitz, and R. N. Zare, J. Chem. Phys. **83**, 2538 (1985).
[7] J. P. Booth, S. L. Bragg, and G. Hancock, Chem. Phys. Lett. **113**, 509 (1985).
[8] P. M. Johnson and C. E. Otis, Annu. Rev. Phys. Chem. **32**, 139 (1981).
[9] J. Morellec, D. Normand, and G. Petite, Adv. At. Mol. Phys. **18**, 97 (1982).
[10] D. C. Jacobs, R. J. Madix, and R. N. Zare, J. Chem. Phys. **85**, 5469 (1986).
[11] V. S. Letokhov, V. I. Mishin, and A. A. Puretzky, Prog. Quantum. Electron. **5**, 139 (1977).
[12] S. Swain, J. Phys. B **12**, 3201 (1979).
[13] D. S. Zakheim and P. M. Johnson, Chem. Phys. **46**, 263 (1980).
[14] J. R. Ackerhalt and B. W. Shore, Phys. Rev. A **16**, 277 (1977).
[15] I. Schek and J. Jortner, Chem. Phys. **97**, 1 (1985).
[16] J. P. Booth, Thesis, Exeter College, Oxford, 1984.

[17]The treatment of C_{01} as a constant assumes that the bandwidth of the laser can be approximated by a rectangular spectral profile, i.e., C_{01} is independent of detuning. Although this does not seem experimentally realistic, a numerical calculation similar to that outlined in Appendix A was performed on the system assuming a Gaussian spectral profile of area C_{01}. The calculated ion yield from the Gaussian pulse was compared to that found by Eqs. (2)–(4) using a scaled constant C_{01}. In a practical experimental regime ($k_{01} \gg k_{12}$ and $k_{01} I \Delta t \approx 2$) the deviation between the two different calculations was less than 3% even when the magnitude of $C_{01} I \Delta t$ was allowed to decrease by an order of magnitude. It is noted that in common practice, there is an undetermined averaging over spectral characteristics of the laser pulse, and it is necessary to assume some type of spectral distribution. The approximation of a flat spectral distribution over the line profile often suffices.

[18]A. C. Kummel and R. N. Zare, J. Chem. Phys. (in press).

[19]R. Altkorn and R. N. Zare, Annu. Rev. Phys. Chem. **35**, 265 (1984).

[20]U. Fano and Joseph H. Macek, Rev. Mod. Phys. Chem. **45**, 553 (1973).

[21]C. H. Greene and R. N. Zare, J. Chem. Phys. **78**, 6741 (1983).

[22]S. N. Dixit and V. McKoy, J. Chem. Phys. **82**, 3546 (1985).

[23]A. R. Edmonds, *Angular Momentum in Quantum Mechanics* (Princeton University, Princeton, 1974).

[24]C. H. Greene and R. N. Zare, Annu. Rev. Phys. Chem. **33**, 119 (1982).

[25]C. H. Townes and A. L. Schawlow, *Microwave Spectroscopy* (McGraw–Hill, New York, 1955).

[26]The product $k_{01} I \Delta t$ is a useful indicator for the degree of saturation in the resonant step. For a system where $k_{01} I \Delta t = 1$, the respective populations in the ground and intermediate states would be 0.57 and 0.43, in the limit where the depletion of population for the intermediate state is due solely to stimulated emission back to the ground state (i.e., ionization and spontaneous emission rates are small).

[27]A. Buckingham, B. Orr, and J. Sichel, Philos. Trans. R. Soc. London Ser. A **268**, 147 (1970).

[28]Y. Itakawa, Chem. Phys. **28**, 461 (1978).

[29]S. Dixit and P. Lambropoulos, Phys. Rev. A **27**, 861 (1983).